Biosensors and Bioelectronics 261 (2024) 116418

Contents lists available at ScienceDirect

Biosensors and Bioelectronics

journal homepage: www.elsevier.com/locate/bios

Array-wide uniform PEDOT:PSS electroplating from potentiostatic deposition

Yieljae Shin, Jaehyeon Ryu, Tianyu Bai, Yi Qiang, Yongli Qi, Gen Li, Yunxiang Huang, Kyung Jin Seo **, Hui Fang *

[a] Thayer School of Engineering, Dartmouth College, Hanover, NH, 03755, USA

ARTICLE INFO

Keywords:
Large scale
Microelectrode array
PEDOT:PSS
Uniformity
Potentiostatic

ABSTRACT

Electroplating of poly(3,4-ethylenedioxythiophene) polystyrene sulfonate (PEDOT:PSS) is important in many neuroelectronic applications but is challenging to achieve uniformity on large-scale microelectrode arrays (MEA) using conventional galvanostatic methods. In this study, we address this challenge through a potentiostatic method and demonstrate highly uniform electroplating of PEDOT:PSS on MEA with more than one hundred electrodes, all at cellular sizes. The validation of this approach involves comparisons with galvanostatic deposition methods, showcasing unparalleled deposition yield and uniformity. Systematic electrochemical characterizations reveal similarities in structure and stability from potentiostatic deposited coatings. The advances developed here establish the potentiostatic method and detailed process to achieve a uniform coating of PEDOT:PSS on large-scale MEA, with broad utility in neuroelectronics.

1. Introduction

Bioelectricity plays a vital role in the brain (Levin, 2023; Hong and Lieber, 2019), possessing rich spatiotemporal dynamic (Townsend and Gong, 2018) that necessitate the use of a large-scale MEA for advanced interfacing (Berdondini et al., 2009). These electrodes facilitate the recording of signals from multiple locations within the targeted tissues (Tian et al., 2023; Chung et al., 2019; Konerding et al., 2018; Lee et al., 2022; Viventi et al., 2011). For instance, the Neuropixel device has been recognized for its capacity to record from thousands of sites, enabling extensive single-unit recordings and brain activity mapping (Steinmetz et al., 2021). Clinical trials involving the Utah array with nearly one hundred microelectrodes have showcased its potential to empower patients in controlling prosthetic devices by neuronal signal interpretation and stimulation (Hochberg et al., 2012). Electrocorticography (ECoG) electrode arrays are instrumental in epilepsy treatment (Xie et al., 2017), and recently, ECoG arrays with hundreds of microelectrodes have enabled speech synthesis by decoding brain signals of spoken sentences (Angrick et al., 2019).

For microelectrodes, it's imperative to attain a coating of low-impedance materials to ensure high-quality electrode recording (Ludwig et al., 2006; Neto et al., 2018). Several low-impedance coatings, including Iridium Oxide (Cogan et al., 2009), Nanostructured Platinum (Boehler et al., 2015), Platinum–Iridium (Petrossians et al., 2011), Titanium Nitride (Meijs et al., 2015), and PEDOT:PSS (Cui and Zhou, 2007) have been explored. Notably, PEDOT:PSS stands out uniquely due to its exceptional biocompatibility (Miriani et al., 2008), electrochemical property (Wang et al., 2021), and adjustable conductivity (Sanviti et al., 2022) when compared to other materials.

For decades, various deposition methods have been investigated for PEDOT:PSS. For instance, spin coating (Illakkiya et al., 2018; Cho et al., 2022) could achieve high electrical conductivity and optical transparency with PEDOT-based polymers. However, spin coating is known to be limited to flat substrates and is prone to easier delamination of the film. Inkjet printing is also a recognized method for coating PEDOT-based polymers (Lo et al., 2021), but its effectiveness is contingent upon the physicochemical properties of the ink and requires a longer coating time. Another method is electrospinning, which recently showed PEDOT:PSS nanofiber coating with high electrical conductivity (Bessaire et al., 2017). However, achieving scalability with this methodology still poses challenges. Electroplating is extensively recognized as an effective and reliable method for the deposition of low-impedance materials on microelectrodes, typically utilizing a three-electrode system. Electroplating is further conducted under three

* Corresponding author.
** Corresponding author. Present address: Science Corporation, Alameda, CA, 94501, USA.
E-mail addresses: kjseo22@gmail.com (K.J. Seo), hui.fang@dartmouth.edu (H. Fang).

https://doi.org/10.1016/j.bios.2024.116418
Received 30 January 2024; Received in revised form 4 April 2024; Accepted 20 May 2024
Available online 21 May 2024

modes, namely potentiostatic (constant potential), galvanostatic (constant current), and cyclic voltammetry (voltage sweeping). This method facilitates meticulous regulation of the coating's thickness and composition, offers a straightforward process, and requires minimal deposition time. Additionally, it is adaptable for versatile sample configurations, regardless of their physical forms.

While numerous studies have explored the electroplating of PEDOT-based polymers, the exploration of electroplating methods in existing literature often focuses on single electrodes, overlooking the complex dynamics of array-wide deposition essential for MEAs. Studies by Tran et al. (2023), Mousavi et al. (2023) and Teixeira et al. (2022) provide valuable insights into the electrodeposition kinetics and physicochemical characteristics of conducting polymers like PEDOT:PSS. Still, they are conducted on single electrodes or bulk substrates rather than on large-scale MEAs. MEA-level electroplating studies exist, but they usually lack emphasis on electrodes with sizes at the cellular level. For instance, Castagnola et al. (2013), Ji and Wang (2020), and Pranti et al. (2018) have contributed significantly to the field by enhancing the electrochemical properties and biocompatibility of electrode surfaces; however, their investigations predominantly utilized electrodes with sizes orders of magnitude larger than cellular dimensions. This size difference underscores a critical gap, as larger electrode windows compromise spatial resolution, making them less effective for precise neuronal spike detection in highlighting the need for cellular-level electrode precision to enhance signal-to-noise ratio (SNR) (Viswam et al., 2019). Aqrawe et al. (2019) and Jones et al. (2020) have involved smaller electrodes and delved into the intricacies of electrode morphology including complex 3D structures, but a detailed investigation of scalability and uniformity across entire microelectrode arrays during electroplating processes remains missing. This gap hints at an overlooked opportunity to deepen our understanding and innovation in the realm of MEA design and fabrication.

To our knowledge, we present the first study focused on (1) array-wide uniform electroplating of PEDOT:PSS on large-throughput (>100 ch) MEAs, with electrode size down to cellular level; (2) comparison of similarities and differences between potentiostatic and galvanostatic electroplating methods in the deposition PEDOT:PSS on large-scale MEAs; (3) understanding of the electrochemical origin of the array-wide uniformity and better scalability from potentiostatic electroplating method. By addressing all the key points highlighted above, our study aims to significantly advance the understanding and application of electroplating in MEAs.

2. Materials and methods

2.1. Device fabrication

To fabricate the substrate, 3 × 2 inch^2 glass was cleaned and blow-dried. Polydemethylsiloxane (PDMS, 10:1 ratio) was spin-coated and cured at 90 °C. Kapton (1 mil thick, Fralock) was laminated, and polyimide (PI 2545, HD MicroSystems) was spin-coated (2 μm thick), cured at 110 °C for 3 min, 150 °C for 5 min, and 250 °C for 70 min. Metals (Cr: 5 nm, Au: 100 nm thick) were deposited via an E-beam evaporator. After deposition, micropatterning was done by photolithography (M400, Midas Systems) using positive photoresist (PR, S1805 G2, MicroChem). Negative PR was spin-coated and patterned as an encapsulation layer (SU-8 2005, Kayaku) and hard baked at 180 °C for 30 min. A laser cutter (U4, LPKF) defined outline of the sample, then the device was peeled off from the PDMS layer.

2.2. Electrochemical deposition of PEDOT:PSS

DI water (100 ml) was mixed with 3,4-Ethylenedioxythiophene (EDOT) monomer (0.1 % (w/v) 0.01 M, Sigma Aldrich) and poly (sodium-4-styrene sulfonate) powder (PSSNa, 0.7 % (w/v), Sigma Aldrich) to make precursors. After 3 h of mixing with a magnetic stirrer, the beaker was left in ambient air for an hour to settle down the precipitates. Silver paste (Ted Pella) was pasted gently on the pad area and dried. The copper tape was taped on the edge to have good contact with the potentiostat. Before soaking the device into the solution, gentle O_2 plasma (100 W, 1 min) treated the device to have improved water wettability, then connected to a three-electrode system with a potentiostat (Reference 620, Gamry), using a platinum wire (0.5 mm diameter, Sigma Aldrich) as the counter electrode (CE) and an Ag/AgCl reference electrode (RE). Potentiostatic function was used for electroplating PEDOT:PSS with a certain amount of time. After deposition, the device was rinsed and blow-dried, removing excess silver paste and copper tape by swabbing in acetone bath.

2.3. Array connection

In-house fabricated printed circuit boards (PCB) were used to connect the Intan headstage (RHS 32 ch, Intan technologies) to the electrodes. The device pads were aligned to the PCB connector and assembled in a fixed position by sandwiching with soft silicone polymers (Ecoflex 0020, Smooth-on) and an acylate top board. Screws and nuts were assembled to secure the location on every corner of the top board. The PCB is soldered with 32 channel connectors (A79022-001, Omnetics), which could be assembled with the head stage later to measure the device impedances.

2.4. Surface analysis

Digital Optical microscope (VHX-7000N, Keyence) was used to take sample images and check uniformities across the whole sample. Scanning electron miscocopy (SEM, Helios 5 CX DualBeam, Thermo Fisher Scientific) was used to take the sample surface morphology by using secondary electron (SE) mode. To measure the array impedances, Intan RHS (Stim/Recording system, Intan technologies) was used. For single-electrode Electrochemical impedance spectroscopy (EIS) measurement, potentiostat (Reference 620, Gamry) was used with a 3-electrode system, and the result was analyzed by software (Framework, Gamry). Origin Pro software was used to generate graphs and heatmaps.

2.5. Accelerated aging test

PEDOT:PSS samples were prepared and soaked in phosphate-buffered saline (PBS). After positioning, the beaker containing PBS was sealed with Kapton film (0.25 mil thick, Durafilm). The beaker was put in the oven and kept at 67 °C. After soaking, the sample was taken out and cooled down to ambient temperature. After cooling down, the sample was taken out from the beaker and rinsed with DI water. The sample was then reassembled with a PCB, and impedance was measured.

3. Result and discussion

3.1. MEA preparation and PEDOT:PSS deposition

We fabricated arrays of 16, 64, and 128 microelectrodes (electrode pitch of 400 μm) and performed PEDOT:PSS deposition using potentiostatic electroplating. Each electrode opening size was set to 10 × 20 μm^2 for this study. Potentiostatic deposition was conducted by applying a constant potential (with reference to a standard Ag/AgCl electrode) to all microelectrodes on a given array, where we temporarily short all contact pads by acetone-removable silver paste. We have determined the specific potential to be the optimal condition through prior experimentation. 0.85 V potential was selected to finely tune the electroplating deposition rate, which is presumably crucial for the coating's morphology and adhesion. This decision was guided by our observations that at 0.8 V, marking the onset of EDOT oxidation and polymerization on the working electrode (Marzocchi et al., 2015; Teixeira et al., 2022), the deposition rate was minimal. Conversely, at 0.9 V, the deposition

rate became excessively high, making it challenging to control the rate of deposition effectively. Optical microscopic images for both conditions are shown in Fig. S1.

Fig. 1 visualizes PEDOT:PSS electroplating methods on a large-scale MEA, compares potentiostatic and galvanostatic approaches, and assesses their scalability. Fig. 1a presents a schematic representation of the electroplating process for PEDOT:PSS on microelectrode arrays (MEAs) using a three-electrode system. Here, two representative modes for electroplating were illustrated. In potentiostatic deposition, constant potential difference between WE and RE is controlled. Conversely, galvanostatic deposition pivots on the control of current, ensuring a steady current flow between the WE and CE. To highlight the advantage of the potentiostatic deposition approach, we compared the potentiostatic and galvanostatic methods with 128-ch arrays of the same design (Fig. 1b–e). In Fig. 1b, an optical microscopic image of 128-ch (32 × 4 matrix) is exhibited along with the images of electrodes on every 10th column. The potentiostatic deposition was carried out at 0.85 V and for 20 s, while the galvanostatic method used a 0.2 mA/cm^2 current density, a typical value for PEDOT:PSS coating on microelectrodes (Qiang et al., 2018). To compare these two methods fairly, we controlled the deposition charge density to be the same. Here, while potentiostatic samples showed electrodes with very similar colors of PEDOT:PSS for all electrodes, the galvanostatic samples did not show uniform coatings. As a result, the mean- impedance of the microelectrodes from these two methods is similar after the deposition, achieving ~100 kΩ and ~120 kΩ, respectively, for the potentiostatic and galvanostatic methods. However, the galvanostatic deposited microelectrodes are much less uniform. The standard deviation values were 29.8 kΩ and 168.29 kΩ, for potentiostatic and galvanostatic methods, respectively, showing ~5.5 × difference. Furthermore, there are many electrodes with impedances over 600 kΩ, which is not suitable for high-performance neural interfacing. Therefore, potentiostatic methods achieve much better uniformity for large-scale MEAs. To add statistical powers, we tested more samples (n = 4) for each condition (Fig. 1f). As a result, their average

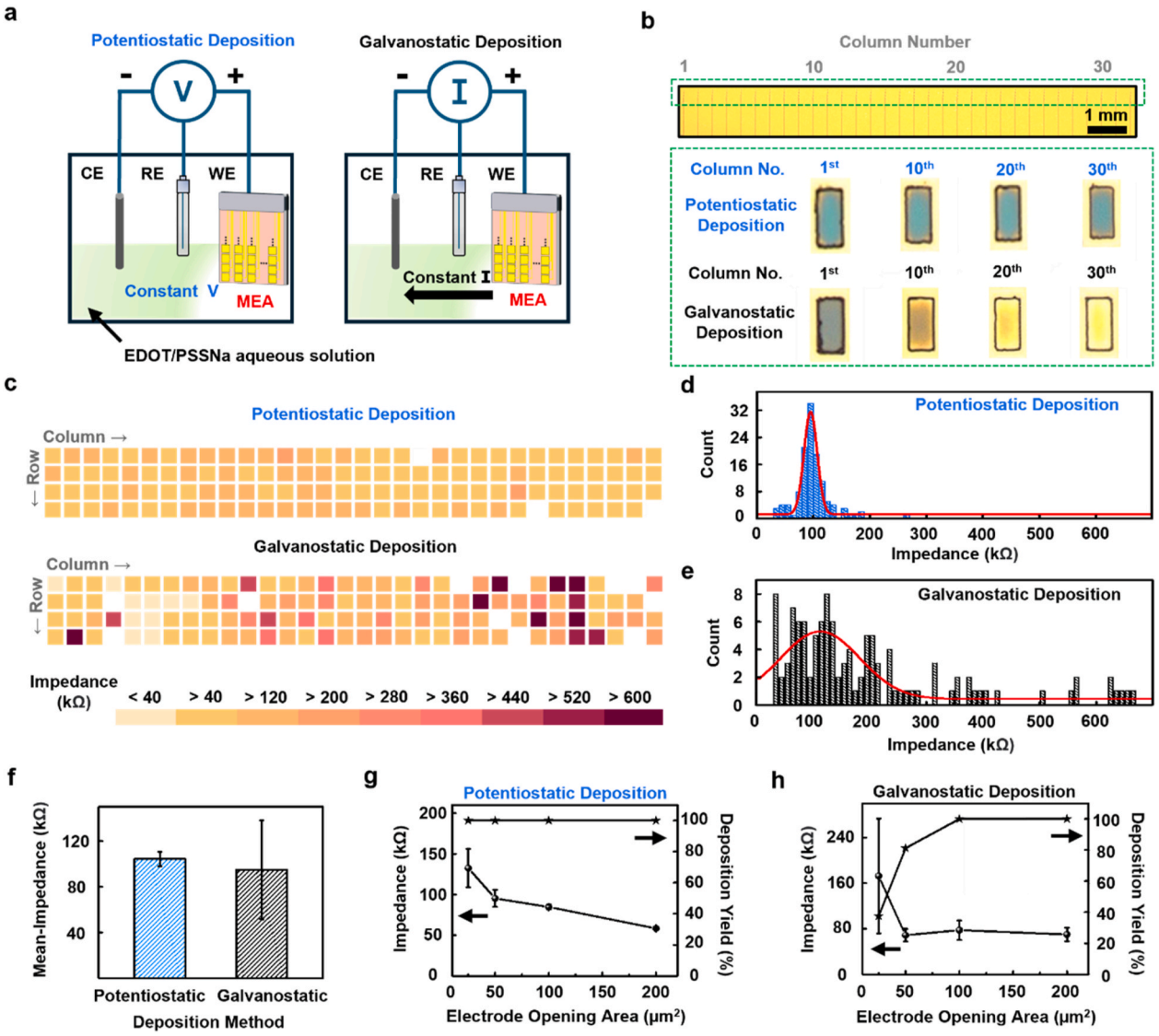

Fig. 1. Demonstration of PEDOT:PSS electroplating on a large-scale MEA and scalability test results. (a) Illustration of PEDOT:PSS electroplating in 3-electrode system and schematics of current density for potentiostatic and galvanostatic deposition in large-scale MEAs. (b) Optical microscopic image of 128-ch MEA with magnified images (× 400) of electrodes after electroplating. Electrode area: 10 × 20 μm^2. (c) Impedance heatmap for potentiostatic deposition and galvanostatic deposition method. (d) Impedance histogram from potentiostatic deposition. (e) Impedance histogram from galvanostatic deposition. (f) Average mean-impedance (Gaussian fitting) of 128-ch MEA based on deposition methods. (g) Impedance and deposition yield (cut-off impedance: 500 kΩ) over various electrode opening areas in potentiostatic deposition, Electrode area: 5 × 5, 5 × 10, 10 × 10, 10 × 20 μm^2. (h) Impedance and deposition yield over various electrode opening areas in galvanostatic deposition.

mean-impedances were similar (104.31 kΩ and 94.95 kΩ for potentiostatic and galvanostatic deposition, respectively), yet the standard deviation values were notably different (6.39 kΩ and 43.18 kΩ, respectively). This result implies that although the amount of deposition was similar, there was a significant difference in uniformity. Lastly, the scalability test was conducted using MEAs with electrode window sizes of 5 × 5, 5 × 10, and 10 × 10 μm^2 (Fig. 1g–h) for both deposition methods. All samples prepared using potentiostatic deposition were processed under the conditions of 0.85 V for a 20-s deposition time. Conversely, samples created through galvanostatic deposition were ensured to get the same charge density. Potentiostatic deposition demonstrated superior uniformity, achieving a 100% deposition yield (percentage of electrodes successfully coated, cut-off impedance of electrode at 1 kHz: 500 kΩ) and an average impedance of 132.45 kΩ with a standard deviation of 23.64 kΩ at 5 × 5 μm^2. On the contrary, galvanostatic deposition at the same size showed less uniformity (deposition yield: 37.5 %), with an average impedance of 172.65 kΩ and a higher standard deviation of 100.74 kΩ, indicating non-uniform coating of PEDOT:PSS. This indication was further vindicated by optical microscopic images (Fig. S2). These results highlight potentiostatic deposition's effectiveness for extremely scaled microelectrodes, essential for high-density neuroelectronic interfaces. Note that for Fig. 1 b-h, all impedance values were collected at 1-kHz-frequency.

To understand the difference between the two methods in depth, we examined the fundamental principles underlying the coating process in electroplating. To start with, we elaborate on the oxidation process of EDOT monomers and the deposition mechanism. The electroplating process initiates with the oxidation of EDOT monomers at the working electrode under a specifically applied voltage. This oxidation results in the formation of two activated monomers that subsequently react, release protons, and generate positively charged PEDOT chains. The negatively charged PSS ions crosslink with these PEDOT$^+$ chains, creating an electrostatically stable bipolymer film, as outlined by Mousavi et al. (2023). For potentiostatic deposition, in addressing the optimal conditions for voltage application during electroplating, we leveraged the Butler-Volmer equation (1), which correlates the electrical current during electroplating with the applied voltage on the electrode.

$$j = j_0 \bullet \left\{ exp\left[\frac{\alpha_a z F}{RT}\left(V - V_{eq}\right)\right] - exp\left[-\frac{\alpha_c z F}{RT}\left(V - V_{eq}\right)\right]\right\} \quad (1)$$

Here, j is the electrode current density, j_0 is the exchange current density, which reflects the rate of an electrochemical reaction at equilibrium when the activation overpotential (V-V_{eq}) is 0. V is the applied potential at the electrode, whereas V_{eq} is the equilibrium potential. α_c is the cathodic charge transfer coefficient and α_a is the anodic charge transfer coefficient which equals to $1 - \alpha_c$. z is the number of electrons involved in the electrode reaction, F is the Faraday constant, and R is the universal gas constant. This equation considers both anodic and cathodic reactions in one electrode, and the total current density is a sum of currents from both anodic and cathodic reactions. At the low overpotential region, where the applied potential is close to the V_{eq}, the equation could be simplified to:

$$j = j_0 \bullet \frac{zF}{RT}\left(V - V_{eq}\right) \quad (2)$$

, where a linear relationship of overpotential and current density is formed. On the contrary, in high overpotential region, the Butler-Volmer equation is simplified to the Tafel equation, where the activation overpotential is substituted to:

$$V - V_{eq} = \pm A \bullet log_{10}\left(\frac{j}{j_0}\right) \quad (3)$$

, with A as the Tafel slope (Katz, 2022). In this region, the current density increases at a much higher rate than that of the linear region, which is called the Tafel region. In both regions, it is clear that the deposition current density is determined only by the electrode potential for a given deposition reaction at a given temperature. Therefore, for the potentiostatic deposition, due to the fact that all microelectrodes are applied with the same potential because of parallel connection via conductive paste on the MEA pad area, the same current density will be flowing through all microelectrodes during electroplating. Assuming all current contributes to the Faradaic reaction, this result will lead to the same deposition rate of PEDOT:PSS films across all microelectrodes (Niederhoffer et al., 2023). Therefore, array-wide uniform electroplating of PEDOT:PSS on all microelectrodes is achieved.

On the other hand, in galvanostatic deposition, the configuration only controls the total current from the working electrode to the counter electrode. Due to the parallel connection of all microelectrodes, the current density at individual microelectrodes can be different from each other, unlike potentiostatic (Fig. S3). This non-uniform distribution of current density is usually inevitable due to different values of microelectrode impedances across the MEA, possibly originating from electrode-to-electrode variations such as the opening area of electrodes, electrode surface roughness, and interconnect length. Electrodes with higher current density compared to others will deposit PEDOT:PSS faster on their surface. This faster deposition will, in turn, reduce the electrode impedance further and promote more current flow and, hence, deposition, thus creating positive feedback on the deposition. Therefore, in galvanostatic deposition, it would be difficult to achieve deposition uniformity of PEDOT:PSS across the large-scale MEA.

The electrode uniformity and surface color with respect to deposition time under the aforementioned conditions are accompanied by morphological changes observed through SEM analysis. In all instances, deposition progressed independently, with coating evident in all conditions except for 0-s deposition. At 0-s deposition (bare Au electrodes, Fig. 2a), since there was no deposition of PEDOT:PSS, we could only observe the surface of the gold film generated by E-beam evaporation. At 5-s deposition (Fig. 2b), deposition is evident, yet full coverage is not achieved. For the 10-s deposition (Fig. 2c), a complete coating is observed, resulting in an overall color of light green. From SEM, we could see that the surface of the electrode is fully covered with PEDOT:PSS. Here, cauliflower-like grains of coating were starting to form. According to Castagnola et al. (2014), PEDOT-rich regions are observed to be slightly brighter than other areas, enclosed in insulating PSS-rich shells. In 15-s deposition samples (Fig. 2d), the coating exhibits a shift in color to purple. From SEM, we could observe larger grains compared to 10-s deposition, with brighter images. This implies that the electrical conductivity increased with more deposition, possessing more PEDOT-rich morphologies. In the 20-s deposition (Fig. 2e), the color transitioned into dark green. From SEM, the image brightness was lower compared to 15-s deposition. This could be due to the charging effect of polymers, where the surface of polymers becomes less conductive because of excessive deposition even though it is conductive. Therefore, instead of dissipating the charge, it accumulates and shows darker contrast than the sample with previous deposition condition.

3.2. Impedance analysis

From the potentiostatic deposition, it is apparent that the deposition charge increases as a function of increasing deposition time. Fig. 2f presents the impedance values at 1 kHz for a group of 16-ch samples with different amounts of PEDOT:PSS coating, together with the cumulative deposition charge. Before deposition, the bare Au microelectrode exhibits a 1-kHz impedance of approximately 2.5 MΩ for a 200 μm^2 site area. With progressing deposition from 5 to 20 s, the impedance decreases progressively from ~150 kΩ to ~60 kΩ. However, beyond 20 s, there is no tendency for the impedance to experience a significant decrease, as evidenced by remarkably similar values obtained from the 40-s deposition compared to 20 s. Meanwhile, the deposition charge

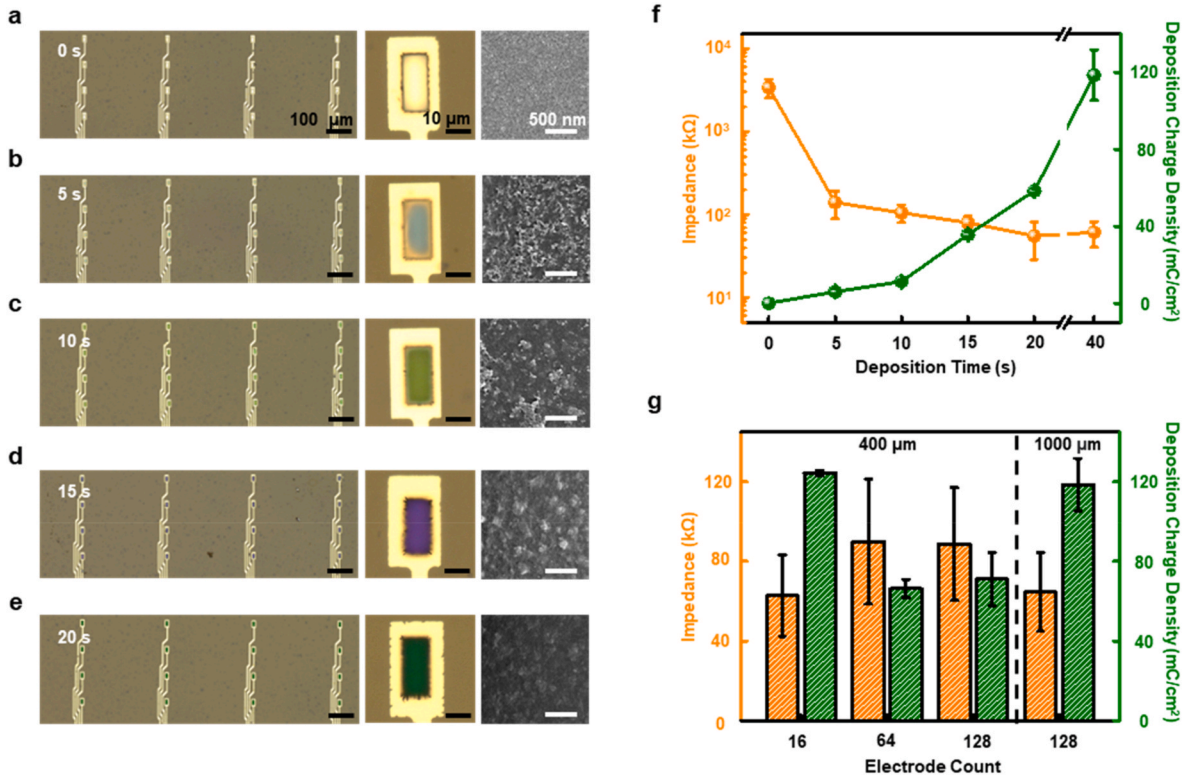

Fig. 2. Optical and electrochemical analysis of MEAs with various potentiostatic deposition times. Optical microscopic and SEM images of MEAs with a deposition time of (a) 0 s (bare Au electrodes), scale bar: 100 μm (left), 10 μm (middle), 500 nm (right). (b) 5 s. (c) 10 s. (d) 15 s. (e) 20 s. (f) Impedance & total deposition charge over various deposition times for 16-ch electrode arrays (0, 5, 10, 15 and 20 s). Deposition potential: 0.85 V. (g) Impedance & total deposition charge over various array configurations (16, 64, 128-ch arrays with 400 μm pitch and 128-ch arrays with a 1000-μm horizontal pitch), with the deposition condition: 0.85 V, 40 s.

density continues to increase over time. This phenomenon indicates that, despite more coating, saturation is eventually observed in impedance (Dijk et al., 2020).

We further investigated the effect of the total number of electrodes on the deposition (Fig. 2g). With the same potentiostatic deposition condition, we observed an electrode number effect where the deposition charge density overall decreases with the increasing electrode number, consequently leading 1-kHz-impedance to increase. This effect is presumably due to the reaction-diffusion process in the electroplating, where the diffusion process will be impacted by the electrode number and affect the overall deposition rate. This hypothesis is further validated by the fact that when comparing 128-ch arrays with a 400 and 1000 μm horizontal pitch, the sample with a 1000 μm pitch had much lower impedance and higher deposition charge. As the electrode density decreases, the EDOT and PSS precursors can more quickly diffuse onto the microelectrodes, where they are consumed during the polymerization process. Although we have not tested the effects of electrode pitch less than 400 μm under the same electrode numbers in galvanostatic deposition, it is speculated that impedance also increases with a decrease in pitch. We expect the same reaction-diffusion competition to happen in galvanostatic deposition when the electrode pitch is reduced. Note in all conditions, uniformity among electrodes was ensured during visual check in the potentiostatic deposition.

3.3. Single electrode electrochemical characterization

To further analyze the properties of the PEDOT:PSS coating from potentiostatic electroplating, EIS and CV measurements were performed from 1 Hz to 1 MHz with single electrodes (n = 4) using a three-electrode setup with a potentiostat. As expected, the impedance decreased significantly as a function of the PEDOT:PSS deposition time, especially between 1 Hz–1 kHz (Fig. 3a). The trend of impedance decrease again slowed down with further deposition, which is consistent with previous observations (Fig. 3a, S4) From the phase spectra perspective, for the frequency below 1 kHz, the phase angle is ~ −90° for all PEDOT:PSS coated cases (Fig. 3b). This phenomenon implies that for this region, the electrode behaves mostly capacitive, and impedance is dominated by the capacitive coupling of the material (Wang et al., 2021). However, at higher frequencies, phase angle value decreases, and this effect is more prominent with longer PEDOT:PSS deposition time. This phase angle change is due to the efficient charge transfer at the PEDOT:PSS-electrolyte interface, lowering the charge transfer resistance. We also prepared and analyzed the EIS of the single electrode sample with the galvanostatic method (Fig. S5). Overall, there is no qualitative difference in impedance or phase spectra comparing the potentiostatic with galvanostatic depositions, indicating similar PEDOT:PSS structures from these two methods. This similarity is not unexpected since the overall methodology of coating is the same electroplating for the two methods.

We also performed CV measurement, scanning between −0.6 V and 0.8 V, with a scan rate of 50 mV/s. As shown in Fig. 3c, PEDOT:PSS deposition onto the Au microelectrode increased its charge storage capacity (CSC), evidenced by the broader enclosed area of the CV curve. This CSC increase continued with more PEDOT:PSS was deposition, reaching ~2.2 mC/cm^2 at 20-s deposition (Fig. 3d). PEDOT:PSS coating tends to have micro- and nano-porous structures, increasing its effective surface area with increasing thickness. For galvanostatic method samples, the CSC value reached ~1.35 mC/cm^2, which is between 5- and 10-s samples of the potentiostatic method. However, the CSC standard deviation of multiple samples from the galvanostatic method is larger (~0.32 mC/cm^2) compared to that of from the potentiostatic method (0.23 and 0.13 mC/cm^2 for 5- and 10-s samples, respectively) due to bigger sample-to-sample variation from the galvanostatic method.

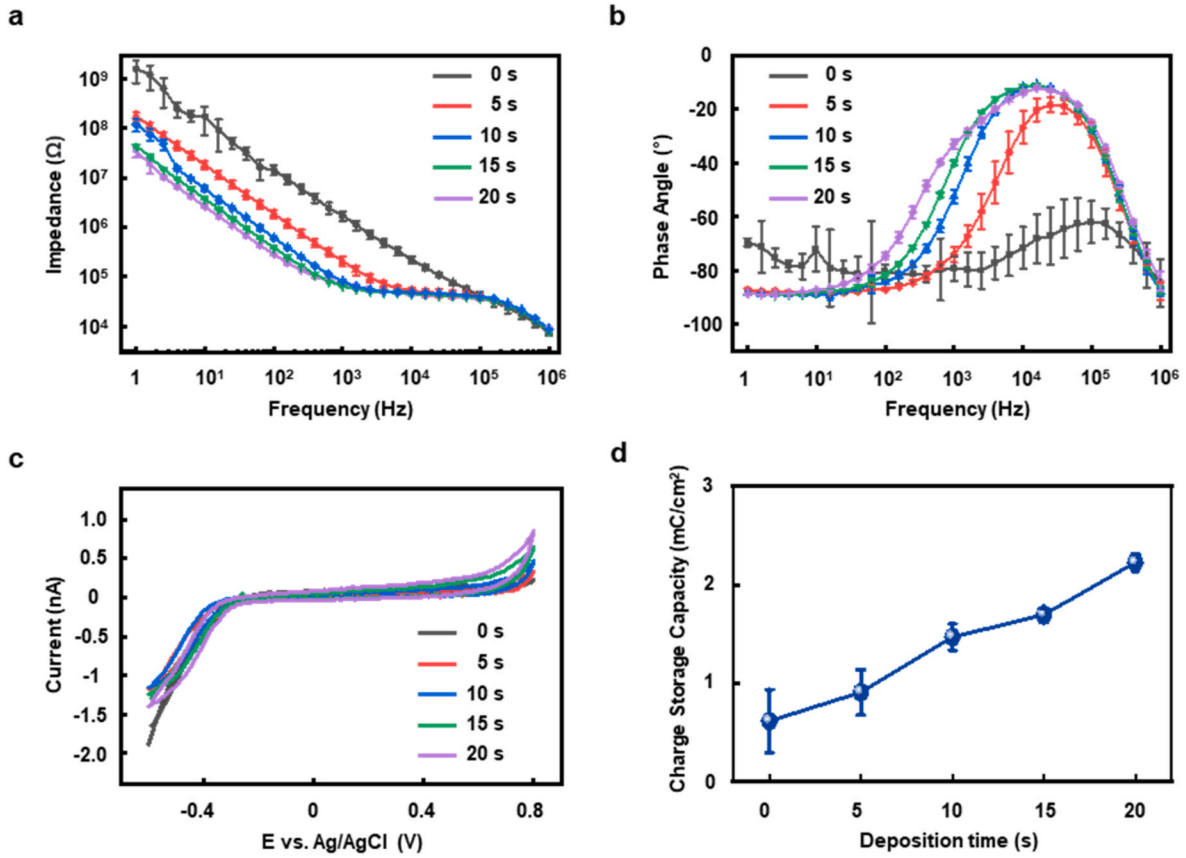

Fig. 3. Single electrode electrochemical characterization as a function of various deposition times (0, 5, 10, 15and 20 s). (a) Bode plot of impedance. (b) Bode plot of phase angle. (c) CV. (d) CSC.

3.4. Chronic stability tests

For many microelectrode applications, chronic stability is important to ensure stable recording and stimulation performance. To this end, we prepared arrays of microelectrodes with potentiostatic PEDOT:PSS deposition and soaked them in PBS to monitor their impedance and yield changes (Fig. 4). We define yield as a percentage of the number of electrodes with measured impedance that does not exceed the cut-off values out of the total number of electrodes. We set the value of the cut-off impedance as 500 kΩ, a typical value in neuroelectronic applications (Park et al., 2014). To accelerate the aging tests, the soaking temperature was set as 67 °C, offering an acceleration factor of 8 compared to 37 °C, assuming an accelerated aging factor Q_{10} of 2 (Hukins et al., 2008). Fig. 4a shows the images of the same electrode by days of soaking, from day 0 to day 9. Here, we used 15-s deposition condition for chronic stability evaluation since this showed the most promising electrochemical performance. More accelerated aging test results are described in Figs. S6 and S7. Through the optical microscope, we observed no delamination or other damage to PEDOT:PSS coating over time, as well as no significant change in the color. These

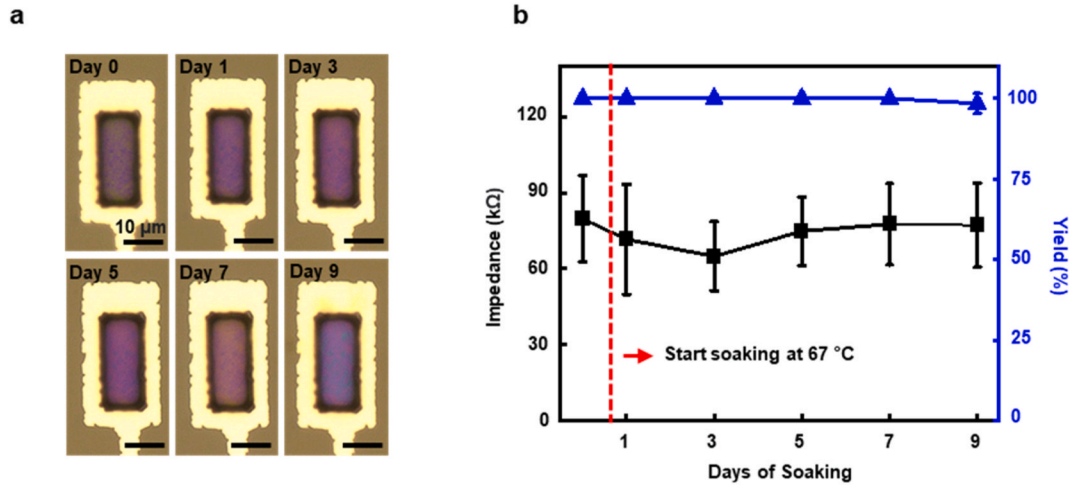

Fig. 4. Chronic stability of PEDOT:PSS with potentiostatic deposition. (a) Optical microscopic images of PEDOT:PSS with 15-s deposition time at different soaking days at 67 °C (scale bar: 10 μm). (b) 1-kHz electrode impedance and array yield (cut-off impedance: 500 kΩ) as a function of soaking days.

observations are consistent with the impedance and yield trends, where both the impedance and array yield remained highly stable over the entire soak duration (Fig. 4b). This stability of 9 days at 67 °C is equivalent to 72 days at 37 °C, suggesting that potentiostatic coated PEDOT:PSS is promising for chronic applications. For the adhesion performance, we compared our results with other research results. Qiang et al. (2018) performed a chronic soak test for 5 weeks in 37 °C PBS, while we demonstrated that we could achieve 8 days in PBS, 67 °C, which is equivalent to 72 days in 37 °C with near 100 % adhesion of the film. Furthermore, our results are similar to Luo et al. (2011) where they performed chronic soaking of the film for 3 months at 37 °C with PEDOT/CNT. Therefore, it is evident that our adhesion is comparable with studies conducted so far.

4. Conclusion

In this study, we have successfully demonstrated (1) the capability of achieving array-wide uniform electroplating of PEDOT:PSS on large-throughput (>100 channels) MEAs with electrode sizes down to the cellular level; (2) a detailed comparison that elucidates the similarities and differences between potentiostatic and galvanostatic electroplating methods in depositing PEDOT:PSS on large-scale MEAs; and (3) a deeper understanding of the electrochemical origins that underlie the array-wide uniformity and enhanced scalability offered by the potentiostatic electroplating method. Furthermore, time-dependent studies revealed that this deposition process is highly controllable, with rates dependent on the electrode throughput and density. From EIS and CV analyses, we found that there was no significant difference in PEDOT:PSS electrochemical properties between the two methods, although galvanostatic deposition samples led to a larger sample-to-sample deviation. Lastly, accelerated aging tests in PBS revealed that PEDOT:PSS from the potentostatic coating was stable for 9 days at 67 °C. Overall, our study established potentiostatic electroplating as a new coating method for large-scale MEA to achieve uniform PEDOT:PSS coating, with broad applications in bioelectronics.

CRediT authorship contribution statement

Yieljae Shin: Writing – review & editing, Writing – original draft, Visualization, Validation, Software, Resources, Methodology, Investigation, Formal analysis, Data curation, Conceptualization. **Jaehyeon Ryu:** Software, Resources, Methodology, Investigation, Formal analysis, Data curation, Writing – original draft. **Tianyu Bai:** Visualization, Resources. **Yi Qiang:** Methodology, Software. **Yongli Qi:** Visualization. **Gen Li:** Formal analysis, Investigation. **Yunxiang Huang:** Resources. **Kyung Jin Seo:** Writing – review & editing, Writing – original draft, Methodology, Conceptualization. **Hui Fang:** Writing – review & editing, Writing – original draft, Project administration, Funding acquisition, Conceptualization.

Declaration of competing interest

The authors declare that they have no known competing financial interests or personal relationships that could have appeared to influence the work reported in this paper.

Data availability

Data will be made available on request.

Acknowledgments

The authors acknowledge support from the National Institutes of Health grant U01NS123668 and RF1NS118301, the National Science Foundation grant 2140392, and the Dartmouth College institutional fund.

Appendix A. Supplementary data

Supplementary data to this article can be found online at https://doi.org/10.1016/j.bios.2024.116418.

References

Angrick, M., Herff, C., Mugler, E., Tate, M.C., Slutzky, M.W., Krusienski, D.J., Schultz, T., 2019. Speech synthesis from ECoG using densely connected 3D convolutional neural networks. J. Neural. Eng. 16 (3), 036019.
Aqrawe, Z., Wright, B., Patel, N., Vyas, Y., Malmstrom, J., Montgomery, J.M., Williams, D., Travas-Sejdic, J., Svirskis, D., 2019. The influence of macropores on PEDOT/PSS microelectrode coatings for neuronal recording and stimulation. Sensor Actuat. B-Chem. 281, 549–560.
Berdondini, L., Imfeld, K., Maccione, A., Tedesco, M., Neukom, S., Koudelka-Hep, M., Martinoia, S., 2009. Active pixel sensor array for high spatio-temporal resolution electrophysiological recordings from single cell to large scale neuronal networks. Lab Chip 9 (18), 2644–2651.
Bessaire, B., Mathieu, M., Salles, V., Yeghoyan, T., Celle, C., Simonato, J.P., Brioude, A., 2017. Synthesis of continuous conductive PEDOT:PSS nanofibers by electrospinning: a conformal coating for optoelectronics. ACS Appl. Mater. Interfaces 9 (1), 950–957.
Boehler, C., Stieglitz, T., Asplund, M., 2015. Nanostructured platinum grass enables superior impedance reduction for neural microelectrodes. Biomaterials 67, 346–353.
Castagnola, E., Ansaldo, A., Maggiolini, E., Angotzi, G.N., Skrap, M., Ricci, D., Fadiga, L., 2013. Biologically compatible neural interface to safely couple nanocoated electrodes to the surface of the brain. ACS Nano 7 (5), 3887–3895.
Castagnola, V., Bayon, C., Descamps, E., Bergaud, C., 2014. Morphology and conductivity of PEDOT layers produced by different electrochemical routes. Synth. Met. 189, 7–16.
Cho, Y.U., Lee, J.Y., Jeong, U.-J., Park, S.H., Lim, S.L., Kim, K.Y., Jang, J.W., Park, J.H., Kim, H.W., Shin, H., Jeon, H., Jung, Y.M., Cho, I.-J., Yu, K.J., 2022. Ultra-low cost, facile fabrication of transparent neural electrode array for electrocorticography with photoelectric artifact-free optogenetics. Adv. Funct. Mater. 32 (10), 2105568.
Chung, J.E., Joo, H.R., Fan, J.L., Liu, D.F., Barnett, A.H., Chen, S.P., Geaghan-Breiner, C., Karlsson, M.P., Karlsson, M., Lee, K.Y., Liang, H.X., Magland, J.F., Pebbles, J.A., Tooker, A.C., Greengard, L.F., Tolosa, V.M., Frank, L.M., 2019. High-density, long-lasting, and multi-region electrophysiological recordings using polymer electrode arrays. Neuron 101 (1), 21–31.
Cogan, S.F., Ehrlich, J., Plante, T.D., Smirnov, A., Shire, D.B., Gingerich, M., Rizzo, J.F., 2009. Sputtered iridium oxide films for neural stimulation electrodes. J. Biomed. Mater. Res. B Appl. Biomater. 89 (2), 353–361.
Cui, X.T., Zhou, D.D., 2007. Poly (3,4-ethylenedioxythiophene) for chronic neural stimulation. IEEE Trans. Neural Syst. Rehabil. Eng. 15 (4), 502–508.
Dijk, G., Ruigrok, H.J., O'Connor, R.P., 2020. Influence of PEDOT:PSS coating thickness on the performance of stimulation electrodes. Adv. Mater. Interfaces 7 (16), 2000675.
Hochberg, L.R., Bacher, D., Jarosiewicz, B., Masse, N.Y., Simeral, J.D., Vogel, J., Haddadin, S., Liu, J., Cash, S.S., van der Smagt, P., Donoghue, J.P., 2012. Reach and grasp by people with tetraplegia using a neurally controlled robotic arm. Nature 485 (7398), 372–375.
Hong, G., Lieber, C.M., 2019. Novel electrode technologies for neural recordings. Nat. Rev. Neurosci. 20 (6), 330–345.
Hukins, D.W., Mahomed, A., Kukureka, S.N., 2008. Accelerated aging for testing polymeric biomaterials and medical devices. Med. Eng. Phys. 30 (10), 1270–1274.
Illakkiya, J.T., Rajalakshmi, P.U., Oommen, R., 2018. Synthesis and characterization of transparent conducting SWCNT/PEDOT: PSS composite films by spin coating technique. Optik 157, 435–440.
Ji, B., Wang, M., 2020. Micro-wrinkle strategy for stable soft neural interface with optimized electroplated PEDOT:PSS. J. Micromech. Microeng. 30 (10), 104001.
Jones, P.D., Moskalyuk, A., Barthold, C., Gutöhrlein, K., Heusel, G., Schröppel, B., Samba, R., Giugliano, M., 2020. Low-Impedance 3D PEDOT:PSS ultramicroelectrodes. Front. Neurosci.-Switz. 14.
Katz, E., 2022. Electrochemical contributions: Julius Tafel (1862–1918). Electrochem. Sci. Adv. 2 (4), e2260002.
Konerding, W.S., Froriep, U.P., Kral, A., Baumhoff, P., 2018. New thin-film surface electrode array enables brain mapping with high spatial acuity in rodents. Sci. Rep. 8 (1), 3825.
Lee, J.Y., Park, S.H., Kim, Y., Cho, Y.U., Park, J., Hong, J.H., Kim, K., Shin, J., Ju, J.E., Min, I.S., Sang, M., Shin, H., Jeong, U.J., Gao, Y.Y., Li, B.W., Zhumbayeva, A., Kim, K.Y., Hong, E.B., Nam, M.H., Jeon, H., Jung, Y., Cheng, H.Y., Cho, I.J., Yu, K.J., 2022. Foldable three dimensional neural electrode arrays for simultaneous brain interfacing of cortical surface and intracortical multilayers. Npj. Flex Electron 6 (1), 86.
Levin, M., 2023. Bioelectric networks: the cognitive glue enabling evolutionary scaling from physiology to mind. Anim. Cogn. 26 (6), 1865–1891.
Lo, L.W., Zhao, J., Wan, H., Wang, Y., Chakrabartty, S., Wang, C., 2021. An inkjet-printed PEDOT:PSS-based stretchable conductor for wearable health monitoring device applications. ACS Appl. Mater. Interfaces 13 (18), 21693–21702.
Ludwig, K.A., Uram, J.D., Yang, J., Martin, D.C., Kipke, D.R., 2006. Chronic neural recordings using silicon microelectrode arrays electrochemically deposited with a poly(3,4-ethylenedioxythiophene) (PEDOT) film. J. Neural. Eng. 3 (1), 59–70.
Luo, X., Weaver, C.L., Zhou, D.D., Greenberg, R., Cui, X.T., 2011. Highly stable carbon nanotube doped poly(3,4-ethylenedioxythiophene) for chronic neural stimulation. Biomaterials 32 (24), 5551–5557.

Marzocchi, M., Gualandi, I., Calienni, M., Zironi, I., Scavetta, E., Castellani, G., Fraboni, B., 2015. Physical and electrochemical properties of PEDOT:PSS as a tool for controlling cell growth. ACS Appl. Mater. Interfaces 7 (32), 17993–18003.
Meijs, S., Fjorback, M., Jensen, C., Sørensen, S., Rechendorff, K., Rijkhoff, N.J., 2015. Electrochemical properties of titanium nitride nerve stimulation electrodes: an in vitro and in vivo study. Front. Neurosci.-Switz. 9.
Miriani, R.M., Abidian, M.R., Kipke, D.R., 2008. Cytotoxic analysis of the conducting polymer PEDOT using myocytes. Annu. Int. Conf. IEEE Eng. Med. Biol. Soc. 2008, 1841–1844.
Mousavi, H., Ferrari, L.M., Whiteley, A., Ismailova, E., 2023. Kinetics and physicochemical characteristics of electrodeposited PEDOT:PSS thin film growth. Adv. Electron. Mater. 9 (9), 2201282.
Neto, J.P., Baião, P., Lopes, G., Frazão, J., Nogueira, J., Fortunato, E., Barquinha, P., Kampff, A.R., 2018. Does impedance matter when recording spikes with polytrodes? Front. Neurosci.-Switz. 12.
Niederhoffer, T., Vanhoestenberghe, A., Lancashire, H.T., 2023. Methods of poly(3,4)-ethylenedioxithiophene (PEDOT) electrodeposition on metal electrodes for neural stimulation and recording. J. Neural Eng. 20 (1), 011002.
Park, D.W., Schendel, A.A., Mikael, S., Brodnick, S.K., Richner, T.J., Ness, J.P., Hayat, M. R., Atry, F., Frye, S.T., Pashaie, R., Thongpang, S., Ma, Z., Williams, J.C., 2014. Graphene-based carbon-layered electrode array technology for neural imaging and optogenetic applications. Nat. Commun. 5 (1), 5258.
Petrossians, A., Whalen, J.J., Weiland, J.D., Mansfeld, F., 2011. Electrodeposition and characterization of thin-film platinum-iridium alloys for biological interfaces. J. Electrochem. Soc. 158 (5), D269–D276.
Pranti, A.S., Schander, A., Bödecker, A., Lang, W., 2018. PEDOT: PSS coating on gold microelectrodes with excellent stability and high charge injection capacity for chronic neural interfaces. Sensor. Actuat. B-Chem. 275, 382–393.
Qiang, Y., Artoni, P., Seo, K.J., Culaclii, S., Hogan, V., Zhao, X., Zhong, Y., Han, X., Wang, P.M., Lo, Y.K., Li, Y., Patel, H.A., Huang, Y., Sambangi, A., Chu, J.S.V., Liu, W., Fagiolini, M., Fang, H., 2018. Transparent arrays of bilayer-nanomesh microelectrodes for simultaneous electrophysiology and two-photon imaging in the brain. Sci. Adv. 4 (9), eaat0626.
Sanviti, M., Martínez-Tong, D.E., Rebollar, E., Ezquerra, T.A., García-Gutiérrez, M.C., 2022. Crystallization and phase separation in PEDOT:PSS/PEO blend thin films: Influence on mechanical and electrical properties at the nanoscale. Polymer 262, 125475.
Steinmetz, N.A., Aydin, C., Lebedeva, A., Okun, M., Pachitariu, M., Bauza, M., Beau, M., Bhagat, J., Böhm, C., Broux, M., Chen, S., Colonell, J., Gardner, R.J., Karsh, B., Kloosterman, F., Kostadinov, D., Mora-Lopez, C., O'Callaghan, J., Park, J., Putzeys, J., Sauerbrei, B., van Daal, R.J.J., Vollan, A.Z., Wang, S., Welkenhuysen, M., Ye, Z., Dudman, J.T., Dutta, B., Hantman, A.W., Harris, K.D., Lee, A.K., Moser, E.I., O'Keefe, J., Renart, A., Svoboda, K., Häusser, M., Haesler, S., Carandini, M., Harris, T.D., 2021. Neuropixels 2.0: a miniaturized high-density probe for stable, long-term brain recordings. Science 372 (6539), eabf4588.
Teixeira, H.J., Dias, C., Veloso, R.C., Apolinário, A., Ventura, J., 2022. Tuning PEDOT: PSS low-impedance thin films with high charge injection for microelectrodes applications. Prog. Org. Coat. 168, 106894.
Tian, Y., Yin, J., Wang, C., He, Z., Xie, J., Feng, X., Zhou, Y., Ma, T., Xie, Y., Li, X., Yang, T., Ren, C., Li, C., Zhao, Z., 2023. An ultraflexible electrode array for large-scale chronic recording in the Nonhuman primate brain. Adv. Sci. (Weinh) 10 (33), e2302333.
Townsend, R.G., Gong, P., 2018. Detection and analysis of spatiotemporal patterns in brain activity. PLoS Comput. Biol. 14 (12), e1006643.
Tran, C.B., Otero, T.F., Travas-Sejdic, J., Le, Q.B., Kiefer, R., 2023. A comparison of poly (3,4-ethylenedioxythiophene) polymerized potentiostatically and galvanostatically. Synth. Met. 299, 117466.
Viswam, V., Obien, M.E.J., Franke, F., Frey, U., Hierlemann, A., 2019. Optimal electrode size for multi-scale extracellular-potential recording from neuronal assemblies. Front. Neurosci.-Switz. 13.
Viventi, J., Kim, D.H., Vigeland, L., Frechette, E.S., Blanco, J.A., Kim, Y.S., Avrin, A.E., Tiruvadi, V.R., Hwang, S.W., Vanleer, A.C., Wulsin, D.F., Davis, K., Gelber, C.E., Palmer, L., Van der Spiegel, J., Wu, J., Xiao, J., Huang, Y., Contreras, D., Rogers, J. A., Litt, B., 2011. Flexible, foldable, actively multiplexed, high-density electrode array for mapping brain activity in vivo. Nat. Neurosci. 14 (12), 1599–1605.
Wang, A., Jung, D., Lee, D., Wang, H., 2021. Impedance characterization and modeling of subcellular to micro-sized electrodes with varying materials and PEDOT:PSS coating for bioelectrical interfaces. Acs Appl. Electron. Mater. 3 (12), 5226–5239.
Xie, K., Zhang, S., Dong, S., Li, S., Yu, C., Xu, K., Chen, W., Guo, W., Luo, J., Wu, Z., 2017. Portable wireless electrocorticography system with a flexible microelectrodes array for epilepsy treatment. Sci. Rep. 7 (1), 7808.